Analytical Methods

ROYAL SOCIETY OF CHEMISTRY

PAPER

View Article Online
View Journal | View Issue

Cite this: *Anal. Methods*, 2021, **13**, 1839

An optic-fiber graphene field effect transistor biosensor for the detection of single-stranded DNA

Yanan Zhang,[a] Yue Ding,[a] Can Li,[a] Huaqiang Xu,[a] Chunxiang Liu,[b] Jingjing Wang,[a] Yong Ma,[a] Junfeng Ren,[ab] Yuefeng Zhao*[a] and Weiwei Yue *[a]

Received 18th January 2021
Accepted 9th March 2021

DOI: 10.1039/d1ay00101a

rsc.li/methods

Herein, a graphene field effect transistor (GFET) was constructed on an optic fiber end face to develop an integrated optical/electrical double read-out biosensor, which was used to detect target single-stranded DNA (tDNA). Two isolated Au electrodes were, respectively, prepared as the drain and source at the ends of an optic fiber and coated with a graphene film to construct a field effect transistor (FET). Probe aptamers modified with fluorophore 6′-carboxy-fluorescein (6′-FAM) were immobilized on the graphene for specific capture of tDNA. Graphene oxide (GO) was introduced to quench 6′-FAM and construct a fluorescence biosensor. Thus, a dual GFET and fluorescence biosensor was integrated on the end-face of an optic fiber. Following synchronous detection by fluorescence and FET methods, results showed satisfactory sensitivity for DNA detection. Compared with conventional biosensors using a single sensing technology, these dual sensing integrated biosensors significantly improved the reliability and accuracy of DNA detection. Furthermore, this proposed technique provides both a new biosensor for single-stranded DNA detection and a strategy for designing multi-sensing integrated biosensors.

1. Introduction

Graphene is a two-dimensional material made of carbon atoms in the shape of a two-dimensional hexagonal lattice.[1] The high carrier mobility and unique band structure of graphene make it extremely useful for FET application. A GFET has the advantages of a FET: fast response time, high sensitivity, low noise, low power consumption, easy integration, a wide safe-working range and so on.[2] It combines the advantages of graphene with higher carrier mobility and better miniaturization potential.[3] As early as 1998, a carbon nanotube FET, a precursor of the GFET, was manufactured.[4] Up to now, GFETs are used to detect physical parameters (such as light, temperature, strain, and magnetic properties), chemical molecules (such as gas molecules, metal ions, and pH), biomolecules (such as DNA, protein, glucose, and bacteria) and even living cells.[5] GFETs were used for label-free detection based on changes in graphene-binding molecules, but not for specific detection of a single molecule. In order to specifically detect a certain molecule, GFETs were generally modified with probe aptamers or enzymes. For example, Kwak *et al.* specifically detected glucose by immobilizing an enzyme that induces a glucose-catalysed reaction on graphene [6] Ohno *et al.* specifically detected immunoglobulin E using a GFET by successfully immobilizing immunoglobulin E aptamers on the surface of graphene,[7] and so on.

Meanwhile, fluorescence resonance energy transfer (FRET) has attracted widespread attention as a technique for fluorescence sensors. Due to its unique conjugated sp^2 structure, graphene and its derivatives can easily combined with fluorescein to quench fluorescein, and can be used as quenchers in FRET.[8] The GO surface has more oxygen-containing groups than graphene, so the quenching efficiency of GO is better than that of graphene. Therefore, GO is widely used as a quencher in various FRET sensors. For example, Wang *et al.* created a FRET sensor that specifically detects adenosine triphosphate (ATP) in living cells,[9] which uses ATP aptamer modified with fluorophores and GO as probe for ATP. The fluorophores on the ATP aptamer is quenched with GO. ATP replaces GO to bind to the ATP aptamer, so the fluorescent group on the ATP aptamer is restored and the amount of ATP in the cell can be measured according to the fluorescence intensity. Jang *et al.* used GO as a quencher to specifically detect the activity of DNA helicase.[10] When DNA helicase is not present, GO cannot quench a fluorophore on single-stranded DNA. Double-stranded DNA is divided into single-stranded DNA when DNA helicase is present. GO quenches the fluorophore on single-stranded DNA. Thus, the presence of DNA helicase can be detected by changes in fluorescence intensity. Nevertheless, despite graphene materials being widely used in biosensors, conventional graphene biosensors commonly exploit only a single graphene characteristic for detection.

[a]*School of Physics and Electronics, Shandong Normal University, Jinan 250014, P. R. China. E-mail: yuewei@sdnu.edu.cn; 176754148@qq.com*

[b]*Institute of Materials and Clean Energy, Shandong Normal University, Jinan 250014, P. R. China*

Multi-sensor integration has been shown to improve reliability for target detection and has been widely used in environmental monitoring, automated target recognition, medical surveillance and biomolecules,[11–14] but there are few reports on the use of multi-sensor integration in graphene biosensors. Herein, we employ multi-sensor integration and exploit the optoelectronic properties of graphene to produce an optic-fiber graphene field effect transistor (OGFET) biosensor integrating a GFET sensor and a FRET sensor. We constructed a GFET on the fiber end face and used graphene combined with a probe aptamer to specifically detect the hybridization of DNA. Meanwhile, due to the superior light transmission of graphene, the fluorophore on the probe aptamer is quenched by GO. The hybridization of DNA is detected by the FRET method. The experimental results show that it is feasible to construct a GFET on the fiber end face and combine the FRET method to detect DNA, and a detection sensitivity of 10 nM can be achieved.

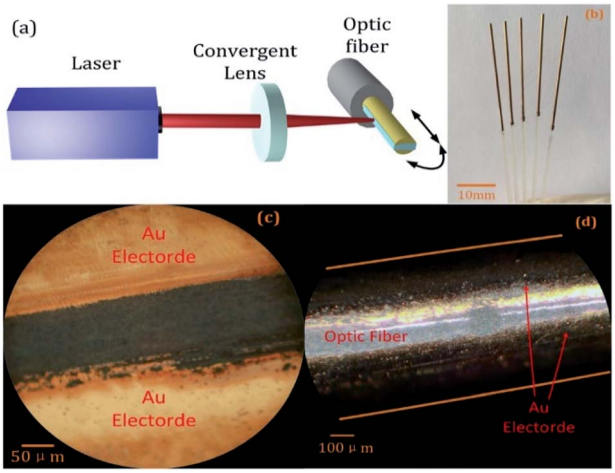

Fig. 1 (a) Schematic of laser etching. (b) Photograph of Au fiber electrodes. (c) End face of the quartz fiber electrode diagram under a 200× objective lens. (d) Fiber side electrode diagram under a 100× objective lens.

2. Experimental

2.1 Reagents and materials

An Ag/AgCl electrode was purchased from Xuzhou Zhenghao Electronic Technology Ltd (China). The amino group and 6′-FAM probe aptamer (sequence: 5′-6′-FAM-ACC TGG GGG AGT ATT GTG GAG GAT CCA-NH_2-3′), complementary tDNA (sequence: 5′-TGG ATC CTC CAC AAT ACT CCC CCA GGT-3′) and mismatched DNA (sequence: 5′-CAT GCA AGT TGA GCG GAC TAT TTC ATC-3′) were purchased from Sangon Biotech Inc (China). 1-Pyrenebutanoic acid succinimidyl ester (PBASE) and dimethyl sulfoxide (DMSO) were purchased from Sigma-Aldrich. Phosphate buffered saline (PBS) was purchased from Sigma-Aldrich. GO was purchased from Nan Jing Xian Feng Nanomaterials Technology Ltd (China). End face flattened fibers (core diameter 400 μm) were purchased from Nan Jing Chun Hui Ltd (China). A magnetron sputtering apparatus was purchased from Denton Vacuum Equipment Ltd (China). A fiber-coupled semiconductor laser was purchased from Yuanming Laser Technology Ltd (China). A photomultiplier tube (PMT), model H9306-04, was purchased from Hamamatsu Photoelectric Ltd (Japan).

The quality of graphene was characterized by Raman microscopy (SPEX-1403, SPEX). A fluorescence spectrophotometer (LS55, PerkinElmer) was used to determine the absorption and emission spectra of the fluorophore labeled on the probe aptamer. A photoelectric double-channel detection system (PEDS) made in the laboratory was used to record the changes in electrical signals and fluorescence signals simultaneously.

2.2 Optic fiber pretreatment and graphene transfer

The first step is the removal of fiber cladding. We removed the cladding of the quartz fiber using an acetone bath (at 60 °C, 20 min). The second step is the plating with a gold film. Au electrodes were prepared by magnetron sputtering (sputtering time 100 s, Au thickness 85 nm, Fig. 1b). Finally, gold electrodes were prepared with a laser etching technique. Previous methods employed for the preparation of isolated Au electrodes as the drain and source electrodes on the fiber end faces have encountered various challenges,[15,16] but the unique characteristics of the laser material interaction mechanism allow laser irradiation to achieve electrode processing.[17] Specifically, according to the thermal effect of the laser and the material, the laser was focused and irradiated on the gold film. Using a rotating platform to rotate the optical fiber as shown in Fig. 1a, isolated gold electrodes could be obtained by laser etching (laser power 800 mW, focusing diameter ~20 μm; Fig. 1a), which were used as drain and source electrodes, respectively. Specifically, we held the fiber in place with a clamp and then moved it under the control of an electric pan. In order to reduce damage to the fiber core, the laser power and movement velocity were optimized while etching the Au film, resulting in the length of the gold film being approximately 30 mm and the distance between the electrodes being approximately 100 μm (Fig. 1c and d). After the Au electrodes were fabricated, a graphene film produced by chemical vapor deposition[18] was transferred and covered on the source and drain electrodes as a conductive channel,[19–21] and the transfer process is shown in Fig. 2. Thus, a GFET was achieved on the optical fiber end.

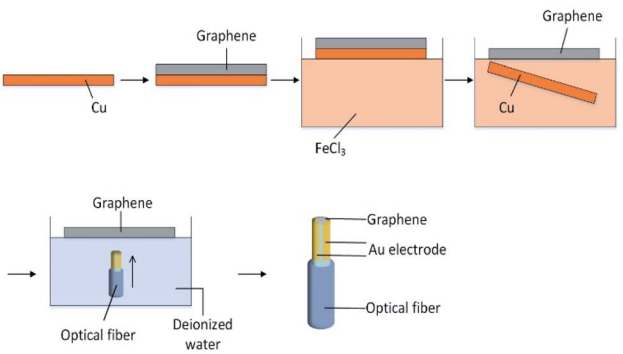

Fig. 2 Process of graphene transfer.

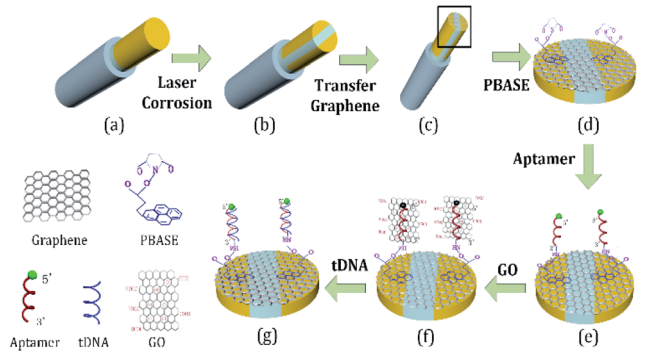

Fig. 3 Fabrication method, modification, and response mechanism of the OGFET.

2.3 Modification and response mechanism of the OGFET

The modification and response mechanism of the OGFET to tDNA are shown in Fig. 3. First, 10 μM PBASE dissolved in DMSO was reacted and incubated on the graphene film at 30 °C for 12 h in an incubator.[22] The OGFET was then washed with DMSO and PBS three times to remove any unbonded PBASE. Due to its pyrene structure, PBASE reacted with graphene through π–π stacking, and the succinimide portion of PBASE was able to immobilize an amine-modified probe aptamer through conjugation between the amine group of the DNA probe and the succinimide group of PBASE.[23] Second, 2 μM probe aptamer dissolved in PBS was added and reacted with PBASE at 30 °C for 2 h. The OGFET was then washed with 2% sodium dodecyl sulfate (SDS) and PBS to remove any unreacted probe aptamers (Fig. 3e). Finally, 100 μg mL^{-1} GO was introduced to quench the 6′-FAM on the probe aptamer. After washing with PBS three times to remove any residual GO, the OGFET biosensor was ready to detect complementary tDNA (Fig. 3f). When tDNA was introduced for detection, the fluorescence of the modified probe aptamer was restored based on FRET (Fig. 3g). Further, the DNA hybridization process modulated the conductivity of the GFET on the optical fiber. Therefore, the fluorescence intensity and the electrical current could be simultaneously detected through a lab-made PEDS (Fig. 4c), constructed as described below.

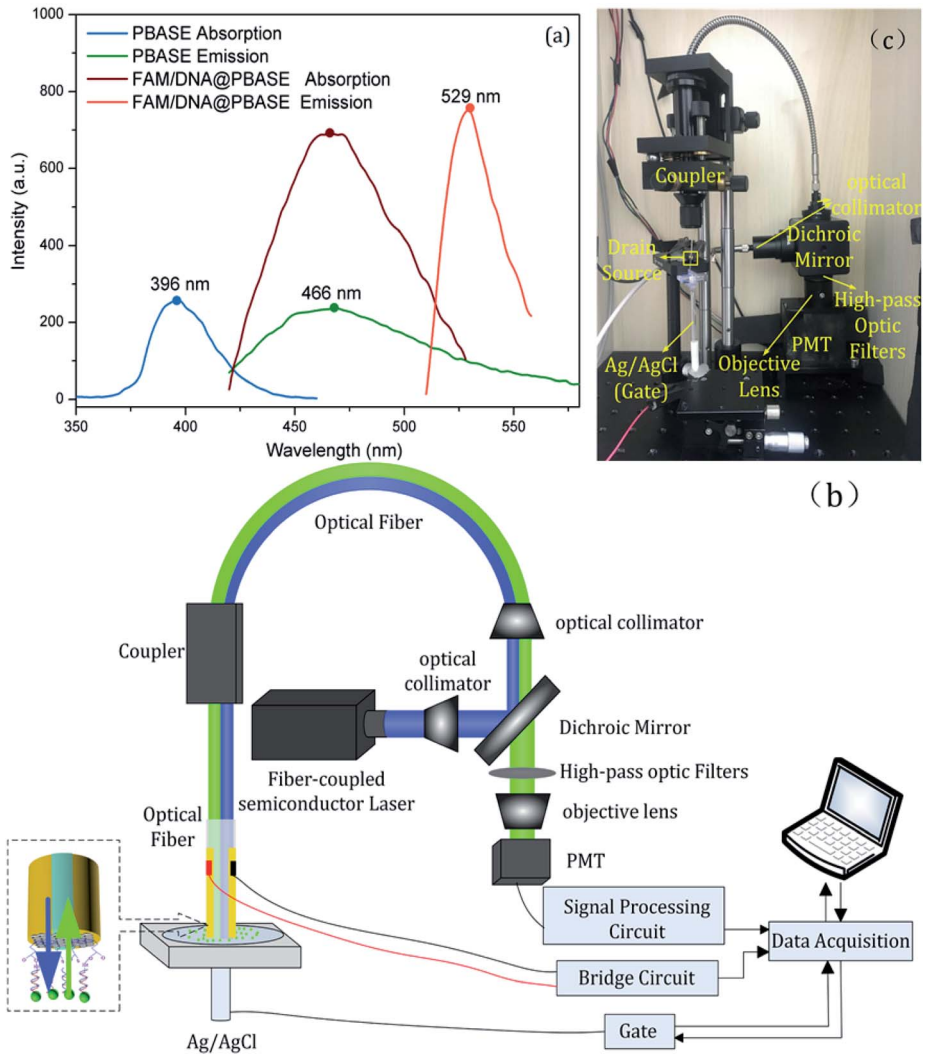

Fig. 4 (a) Absorption and emission spectra of PBASE and the probe aptamer. (b) Schematic diagram of the PEDS. (c) Photograph of the PEDS.

2.4 Construction of the lab-made PEDS

First, Fig. 4b shows a schematic diagram of the lab-made PEDS, which mainly includes an optical unit and an electric unit. The electric unit mainly includes a power module, gate voltage output module, bridge circuit module, PMT gain control module and analog-to-digital signal acquisition module. In order to select suitable optical elements, the absorption and emission spectra of PBASE and the 6′-FAM modified probe aptamer were collected with a fluorescence spectrophotometer as shown in Fig. 4a. Based on the absorption and emission spectra of PBASE and 6′-FAM on the probe aptamer, a fiber-coupled semiconductor laser, with a center wavelength of 465 nm, was selected as the excitation light source. The laser beam output from the fiber-coupled semiconductor laser was collimated and filtered following reflection by a dichroic mirror and optical collimator, and coupled to an optic fiber as the excitation light. Then, the excitation light was coupled directly to the OGFET and the fluorescent group was excited in the presence of tDNA based on FRET. The emitted fluorescent light, with a wavelength of about 525 nm, was collected through the OGFET and detected by a PMT after successively passing through the dichroic mirror and a high-pass optic filter.

Subsequently, the liquid gate voltage (V_g) was generated using a 16 bit digital-to-analog module and applied on the OGFET *via* an Ag/AgCl electrode immersed in the electrolyte as shown in Fig. 4b. The voltage (V_{ds}) between the source and drain OGFET electrodes was recorded directly through the data acquisition unit (Fig. 4b). The OGFET electrical current intensity (I_C) could be calculated through V_{ds}.

Finally, both the intensity of fluorescence (I_F) and I_C of the OGFET were recorded synchronously and uploaded to a computer using a double-channel data acquisition unit (Fig. 4b). The complete image of the PEDS is shown in Fig. 4c.

3. Results and discussion

3.1 OGFET characterization

In this OGFET, on the one hand, the properties of the transferred graphene film had an important influence on the performance of the biosensor.[24] Therefore, the transmittance of the graphene film was recorded using a fluorescence spectrophotometer (LS55, PerkinElmer) (Fig. 5a). As shown in Fig. 5a, both the excitation and absorption transmittances were over 90%, indicating that the light transmittance of graphene films was very good, and the light excitation and emission could not be reduced.[25–27] On the other hand, the quality of graphene transferred to the end face of the optical fiber also has a huge impact on the sensitivity and reliability of the construction of biosensors, so the transfer of high-quality graphene is a necessary condition for the manufacture of biosensors, and the quality of the transferred graphene can be analysed by Raman spectroscopy (SPEX-1403, SPEX) (Fig. 5b).[28] It can be seen from the figure that the Raman spectrum of graphene on the end face of the fiber has three peaks: D band, G band and 2D band. The I_{2D}/I_G intensity ratio can be used to verify the number of graphene layers,[29] and using this, we proved herein that graphene was multilayer. The D band in Fig. 5b presented some defects may be introduced during the process of grahene transfer. After the graphene films were modified with PBASE, the corresponding characteristic peaks appeared at 1233.1 cm^{-1}, 1445.7 cm^{-1}, and 1657.8 cm^{-1}, respectively. Compared with the PBASE peak calculated theoretically, the results are basically consistent. The peak at 1233.1 cm^{-1} was due to sp^3 bonding. The peak at 1657.8 cm^{-1} was assigned to the pyrene group and the peak at 1445.7 cm^{-1} to the disorder arising from the orbital hybridization of the molecule with the graphene film. These results demonstrated that PBASE was modified on the graphene surface as a linker.

Due to the zero band-gap structure[30] and high electron mobility[31] of graphene, the GFET exhibited typical bipolar characteristics centered on the Dirac point (Fig. 6a).[32] The Dirac point also shifted when charged molecules were added to the GFET (Fig. 6b). According to a capacitance model of a GFET,[20,33] we concluded that a Dirac point shift towards the right was observed in the presence of negatively charged molecules and a shift towards the left was observed in the presence of positively charged molecules. Based on this principle, first, we measured the bipolar properties of graphene by adding a pH 7.4

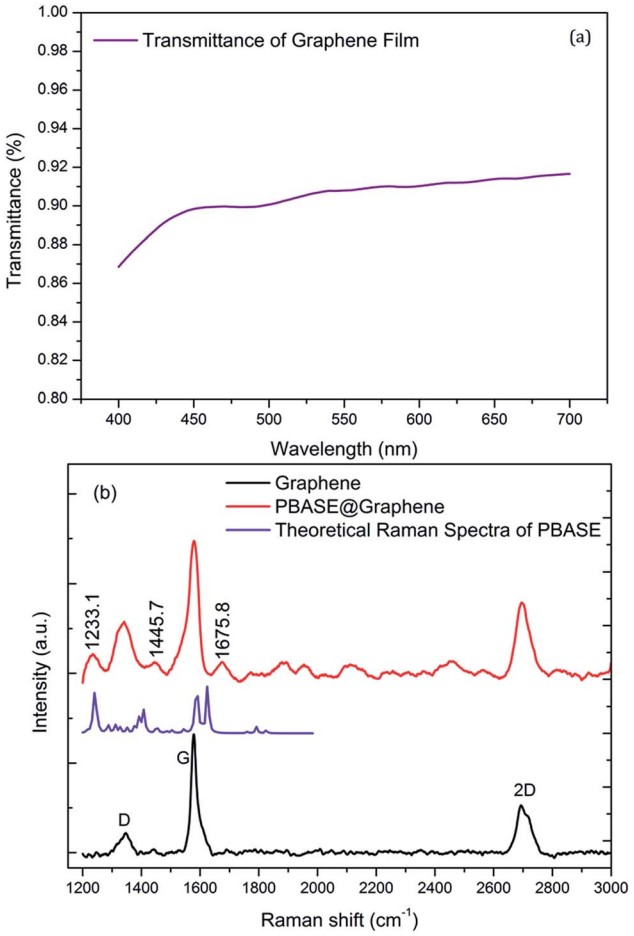

Fig. 5 Characterization of graphene before and after modification with PBASE. (a) Transmittance of the graphene film. (b) Raman spectra of graphene films.

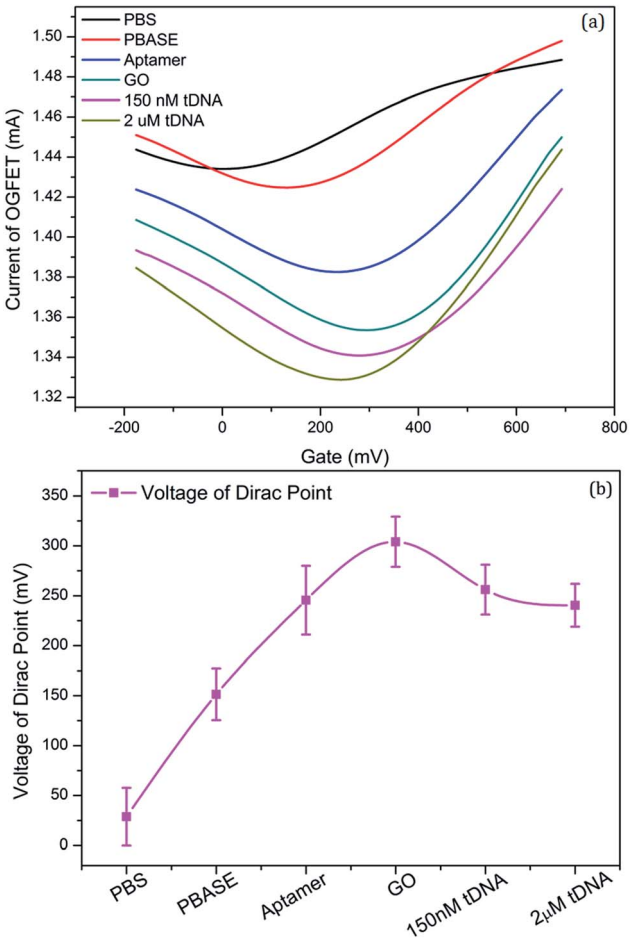

Fig. 6 Dirac point characteristics of the OGFET. (a) Bipolar characteristics of the OGFET. (b) Shift of Dirac points.

PBS solution to the device. Next, after functionalization with PBASE, a probe aptamer and GO solution were added to the device, and changes in the bipolar properties of graphene caused by each charge doping were measured, and as shown in Fig. 6b, the Dirac point shifted to the right. This indicated that the probe aptamer and GO, both of which are negatively charged, were successfully anchored on the graphene through PBASE functionalization. Conversely, with the addition of the tDNA, the Dirac point shifted towards the left, indicating that tDNA replaced GO and hybridized with the probe aptamer, thereby weakening the negative charge modification of the GFET. Because GO has more negative charges than tDNA, after adding 2 μM tDNA, tDNA replaces a larger amount of GO, and the total amount of negative charge decreases, causing the Dirac point to shift towards the left. Additionally, based on the results shown in Fig. 6a, we could also conclude that the electric current in the OGFET under a fixed V_g could be used to detect their modification and the concentration of tDNA samples.

3.2 PEDS detection of the OGFET

First of all, the changes in I_F and I_C generated by the OGFET during the modification process were detected and recorded by using a PEDS with fixed V_g at 100 mV. As shown in Fig. 7, when 2 μM probe aptamer was added to the OGFET, the I_F of the OGFET significantly increased and the I_C significantly decreased. A significant increase in I_F indicated that the probe aptamer modified with 6′-FAM was fixed to graphene, and the significant decrease in I_C in the OGFET was due to the band gap opening to the Fermi energy when foreign molecules were attached to graphene, resulting in a decrease in the conductivity of the graphene absorption system.[34,35] Next, when a GO solution was added to the OGFET, the I_F of the OGFET significantly decreased, and I_C continued to decrease. A significant decrease in I_F confirmed that 6′-FAM on the probe aptamer was quenched based on FRET. The continuous decrease of I_C in the OGFET indicates that GO binds to the probe aptamer. Finally, when tDNA solution was added to the OGFET, the I_F of the OGFET increased significantly and the I_C continued to decrease. An increase in I_F indicated that tDNA replaced GO, resulting in fluorescence restoration of 6′-FAM on the probe aptamer. The I_C decline indicates that tDNA binds to the probe aptamer. In addition, the variation trend of I_C is consistent with the characteristic curve of the OGFET (Fig. 6a). Therefore, the OGFET designed in this study can simultaneously detect the modification of tDNA samples through fluorescence channels and FET channels. Fluorescence channels and FET channels show a consistent trend in detecting tDNA concentration, which will give measurement results that are more accurate and reliable than those of single channels.

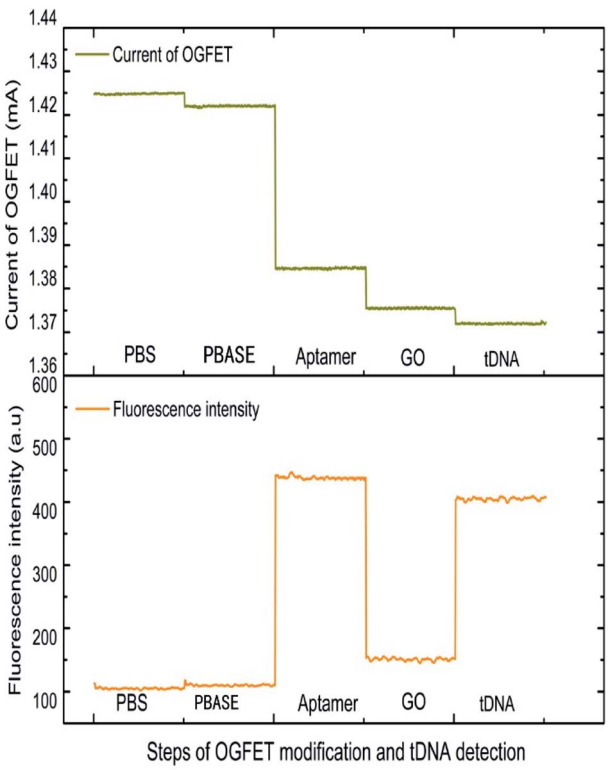

Fig. 7 Fluorescence and current intensity during OGFET modification and tDNA detection.

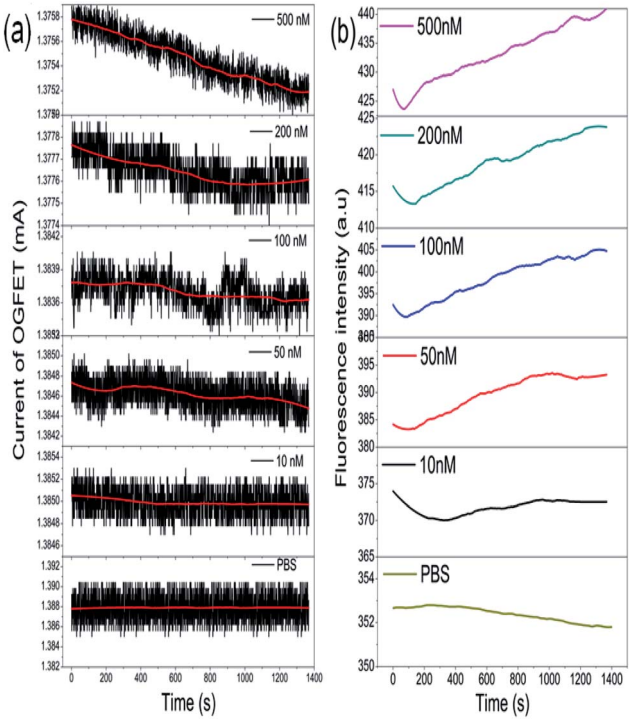

Fig. 8 Comparison of optical detection and electrical detection results. (a) Electrical channel. (b) Fluorescence channel.

3.3 Detection of DNA hybridization

To test the practicability of the OGFET, we examined the binding kinetics of real-time DNA hybridization between different concentrations of tDNA and probe aptamers. First, we added different concentrations of tDNA to the functionalized graphene in the order from low to high. The tDNA concentrations were 10 nM, 50 nM, 100 nM, 200 nM and 500 nM, respectively. Then, I_C and I_F can be obtained simultaneously in real time based on the dual electro-optical sensing characteristics of the OGFET and the real-time monitoring performance of the PEDS (Fig. 8). When different concentrations of tDNA were added, for electrical channels, the I_C of the OGFET gradually decreased and then stabilized (Fig. 8a), indicating that hybridization between the tDNA and the probe aptamer was completed. And the higher the tDNA concentration, the faster the hybridization reaction. For the fluorescence channel, the I_F of the OGFET gradually increased and then stabilized (Fig. 8b), indicating that tDNA had replaced GO and combined with the probe aptamer, and the fluorophore on the probe aptamer was restored. The fluorescence channel and the electrical channel showed a consistent trend in detecting tDNA sensitivity. This will make the measurement results of this sensor more reliable than the measurement results of a single channel sensor, and at the same time, according to this result, it can be seen that the sensitivity of this sensor can reach 10 nM.

3.4 Negative control experiments

We further verified the specificity of the OGFET using mismatched DNA. First, 2 μM mismatched DNA dissolved in PBS solution was placed in the reaction pool for 10 minutes to fully react. The OGFET was then cleaned with 2% SDS and PBS to remove excess mismatched DNA. Finally, as a control experiment, 2 μM matched tDNA was added to the reaction tank and washed again after 10 minutes of reaction. We used the PEDS to monitor the changes of I_C and I_F during the whole reaction process. As shown in Fig. 9a, at the same molality, the I_C of mismatched DNA did not change significantly, but the I_C of matched tDNA decreased significantly. After the reaction, the OGFET was placed in the same PBS solution and the PEDS was used to detect the bipolar properties of graphene. As shown in Fig. 9b, the Dirac point of graphene did not change after the addition of mismatched DNA, indicating that mismatched DNA did not react with the probe aptamer. After the addition of

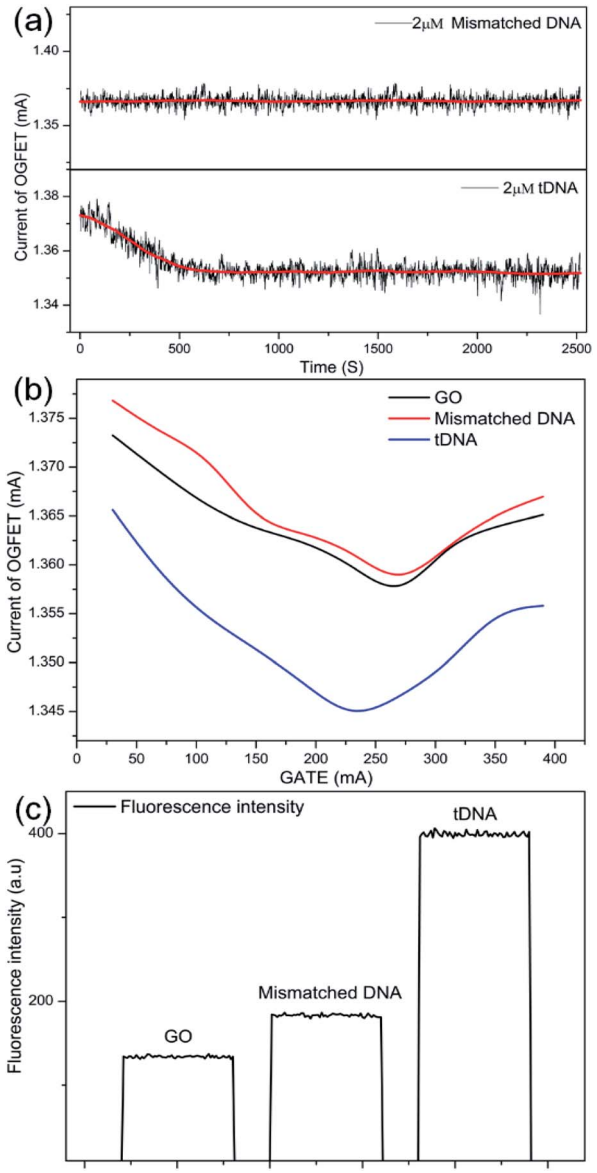

Fig. 9 Negative control experiment. (a) Electric current intensity during OGFET detection. (b) Dirac point characteristics of OGFET detection. (c) Fluorescence intensity during OGFET detection.

matched tDNA, the shift of the Dirac point to the left indicates that matched tDNA replaces GO and binds to the probe aptamer. In addition, changes in I_F also indicate that the OGFET binds only to matched tDNA (Fig. 9c). This experiment proved that the OGFET has excellent specificity.

4. Conclusions

Herein, an OGFET biosensor was developed through the transfer of a graphene film onto the face-end of an optic fiber. Through the magnetron sputtering and laser etching method, Au electrodes were, respectively, prepared on the optic fiber as the source and drain electrodes. Following immobilization of the probe aptamer and GO onto the graphene film, tDNA was captured and detected *via* the GFET and fluorescence methods simultaneously. Through the detection of tDNA, this dual-sensing integrated biosensor not only improves the reliability and efficiency of the detection, but also can be used for the detection of different targets in addition to the detection of the same target. Particularly, based on the non-invasive and penetrating properties of light, the sensor also has the potential to be used for simultaneous detection of different molecules inside and outside the cell, which is of great significance for studying the mechanism of cell activity. Therefore, this work has provided an opto-electrical graphene biosensor for DNA detection as well as a new strategy for the construction of multi-sensing integrated biosensors.

Author contributions

Yanan Zhang, Weiwei Yue and Yuefeng Zhao conceived the concept. Yue Ding and Can Li initiated the sensor design. Yue Ding and Chunxiang Liu prepared Au electrodes *via* laser etching, Yanan Zhang performed the measurements. Huaqiang Xu, Jingjing Wang, Yong Ma and Junfeng Ren analysed the data and wrote the manuscript. All the authors edited, discussed and approved the whole paper.

Conflicts of interest

The authors declare that they have no competing interests.

Acknowledgements

The study was supported by the Natural Science Foundation of Shandong Province (Grant No. ZR2019MF025) and the Foundation of Shandong Provincial Key Laboratory of Biophysics (Grant No. SD2019BP003) and the National Natural Science Foundation of China (Grant No. 11674199, 12074226, and 12074229).

References

1 I. I. Bobrinetskiy and N. Z. Knezevic, *Anal. Methods*, 2018, **10**, 5061–5070.
2 S. Mao, J. Chang, H. Pu, G. Lu and J. Chen, *Chem. Soc. Rev.*, 2017, **46**, 6872–6904.
3 X. Li, R. Xie, L. Fan, W. Zhou, Z. Wang, Y. Liu and Y. Li, *Anal. Methods*, 2016, **8**, 4001–4016.
4 S. J. Tans, A. R. M. Verschueren and C. Dekker, *Nature*, 1998, **393**, 49–52.
5 B. Zhan, C. Li, J. Yang, G. Jenkins, W. Huang and X. Dong, *Small*, 2015, **10**, 4042–4065.
6 Y. H. Kwak, D. S. Choi, Y. N. Kim, H. Kim, D. H. Yoon, S.-S. Ahn, J. W. Yang, W. S. Yang and S. Seo, *Biosens. Bioelectron.*, 2012, **37**, 82–87.
7 Y. Ohno, K. Maehashi and K. Matsumoto, *J. Am. Chem. Soc.*, 2010, **132**, 18012–18013.
8 P. Hu, C. Zhu, L. Jin and S. Dong, *Biosens. Bioelectron.*, 2012, **34**, 83–87.
9 Y. Wang, Z. Li, D. Hu, C. T. Lin and Y. Lin, *J. Am. Chem. Soc.*, 2010, **132**, 9274–9276.
10 H. Jang, Y. K. Kim, H. M. Kwon, W. S. Yeo and D. H. Min, *Angew. Chem.*, 2010, **49**, 5703–5707.
11 Q. Han, X. Zhao, N. Na and J. Ouyang, *Anal. Chem.*, 2021, **93**, 3486–3492.
12 R. J. K. H. Cohen, *Neural Networks*, 1999, **12**, 355–370.
13 X. Gao and A. Levent, *Sensors*, 2016, **16**, 1034–1048.
14 B. Hermans and R. Puers, *Sens. Actuators, A*, 2005, **123**, 423–429.
15 B. C. Zheng, S. C. Yan, J. H. Chen, G. X. Cui, F. Xu and Y. Q. Lu, *Laser Photonics Rev.*, 2015, **9**, 517–522.
16 J. H. Chen, Z. H. Liang, L. R. Yuan, C. Li, M. R. Chen, Y. D. Xia, X. J. Zhang, F. Xu and Y. Q. Lu, *Nanoscale*, 2017, **9**, 3424–3428.
17 K. Venkatakrishnan, B. Tan and K. A. B. Ngoi, *Opt. Laser Technol.*, 2002, **34**, 199–202.
18 D. A. C. Brownson and C. E. Banks, *Phys. Chem. Chem. Phys.*, 2012, **14**, 8264–8281.
19 J. Ma, J. Wei, H. L. Ho and Y. D. Ji, *Opt. Lett.*, 2012, **37**, 2493–2495.
20 S. Xu, B. Man, S. Jiang, J. Wang, J. Wei, S. Xu and H. Liu, *Physics*, 2015, **7**, 146–150.
21 W. Yue, S. Jiang, S. Xu, M. Yong and C. Bai, *Sens. Actuators, B*, 2015, **214**, 204–210.
22 D. Du, S. Guo, L. Tang, Y. Ning, Q. Yao and G. J. Zhang, *Sens. Actuators, B*, 2013, **186**, 563–570.
23 S. Xu, J. Zhan, B. Man, S. Jiang, W. Yue, S. Gao, C. Guo, H. Liu, Z. Li and J. Wang, *Nat. Commun.*, 2017, **8**, 14902–14911.
24 Y. Hernandez, V. Nicolosi, M. Lotya, F. Blighe, Z. Sun, S. De, I. T. Mcgovern, B. Holland, M. Byrne and Y. Gunko, *Nat. Nanotechnol.*, 2008, **3**, 563–568.
25 S. De and J. N. Coleman, *ACS Nano*, 2010, **4**, 2713–2720.
26 R. Gao, D. Lu, J. Cheng and Z. M. Qi, *Opt. Lett.*, 2017, **42**, 2703–2706.
27 S. Luo, Y. Wang, X. Tong and Z. Wang, *Nanoscale Res. Lett.*, 2015, **10**, 199–209.
28 J. B. Wu, M. L. Lin, X. Cong, H. N. Liu and P.-H. Tan, *Chem. Soc. Rev.*, 2018, **47**, 1822–1873.
29 I. Calizo, I. Bejenari, M. Rahman, G. Liu and A. A. Balandin, *J. Appl. Phys.*, 2009, **106**, 043509–043513.
30 Y. Zhu, S. Murali, W. Cai, X. Li, J. W. Suk, J. R. Potts and R. S. Ruoff, *ChemInform*, 2010, **22**, 3906–3924.

31 C. Shen, G. Huang, Y. Cheng, R. Cao, F. Ding, U. Schwingenschlögl and Y. Mei, *Nanoscale Res. Lett.*, 2012, **7**, 268–275.
32 M. Orlita, C. Faugeras, P. Plochocka, P. Neugebauer and M. Potemski, *Phys. Rev. Lett.*, 2009, **101**, 267601–267604.
33 W. Yue, C. Tang, C. Wang, C. Bai, S. Liu, X. Xie, H. Hua, Z. Zhang and D. Li, *RSC Adv.*, 2017, **7**, 44559–44567.
34 F. Liu, J. Y. Choi and T. S. Seo, *Biosens. Bioelectron.*, 2010, **25**, 2361–2365.
35 B. Rosenstein, M. Lewkowicz and T. Maniv, *Phys. Rev. Lett.*, 2013, **110**, 066602–066606.